



MOF Crystals as Precursors

A Facile Synthesis of Co₃O₄ Hollow Microtubes by Decomposition of a Cobalt Metal–Organic Framework

L. Claudia Gómez-Aguirre*^[a] Socorro Castro-García*^[a] Manuel Sánchez-Andújar,^[a]
Susana Yáñez-Vilar,^[a] Jorge Mira,^[b] Juan Manuel Bermúdez-García,^[a] Teresa A. Centeno,^[c]
and María Antonia Señarís-Rodríguez^[a]

Abstract: In this work, we have successfully synthesized hollow microtubular crystals of the metal–organic framework (MOF) [Co₂(NH₂-bdc)₂(dabco)]·[G] {G = H₂O, *N,N*-dimethylformamide (DMF); NH₂-bdc = 2-amino-1,4-benzenedicarboxylate; dabco = 1,4-diazabicyclo[2.2.2]octane} by a very simple coordination-modulation method that avoids the use of an external modulator. Additionally, we have obtained the corresponding hollow microtubular crystals of Co₃O₄ through the solid-state thermol-

ysis of the Co-MOF material at 400 °C. The as-prepared Co₃O₄ crystals exhibit the typical magnetic behavior for a nanostructured material with good crystallinity. Thus, this coordination-modulation method provides a simple route for the preparation of nanostructured porous frameworks and derived oxides and opens a way to prepare new materials with advanced properties.

Introduction

One of the challenges for material scientists is the preparation, control, and manipulation of the size and shape of materials on the nanometer scale to attain new functional properties compared with those of the bulk materials. In particular, one-dimensional (1D) and hollow nanostructures are attracting increased attention owing to their multiple technological applications that range from building blocks for the fabrication of nanoscale electronics and photonics to molecular chemical and biological nanosensors as well as drug delivery systems, catalysts, or energy-storage and conversion materials.^[1,2] For all of these applications, it is very important to have nanomaterials with high specific surface areas to increase their capacities.^[3,4] This is the case, for example, for the well-known Co₃O₄. This mixed oxide has a spinel structure and is an important magnetic p-type semiconductor of interest for many functional applications, including heterogeneous catalysis, solid-state sensors, chemical storage, water treatment, magnetism, anode materials in Li-ion rechargeable batteries, electrochromic devices, solar-energy absorbers, pigments, and even pseudocapacitor electrodes.^[2,5–7] As Wang et al. indicated in a recent review on this oxide,^[2] an

important goal still to be achieved is the design and development of more versatile and powerful synthetic tools for the preparation of new Co₃O₄ hollow structures.

In this context, other systems of interests are metal–organic frameworks (MOFs), which are hybrid inorganic–organic materials consisting of metal atoms or clusters linked by polyfunctional organic ligands to form one-, two-, or three-dimensional structures. These compounds have been studied extensively in the last decade owing to their interesting applications in gas storage and catalysis.^[8] They are receiving more attention as they can display a wide range of other functional properties,^[9] among which are their very recently found dielectric^[10] and even multiferroic properties.^[11,12] Moreover, many of them can be easily transformed into metal oxides through simple calcination or thermolysis. This is a very recent and effective method for the preparation of metal oxide nanoparticles^[13–18] that avoids the use of the structure-directing surfactants needed in some other common synthesis methods.

Despite the advances made in this field in recent years, little progress has been made in the miniaturization of the MOF particle size. Although several approaches have been developed to fabricate MOF nanoparticles through bottom-up self-assembly processes, in general, it is difficult to control the rate of framework extension. In this context, a very interesting synthetic strategy has recently been proposed^[19,20] and involves the selective modulation of the coordination interaction in the framework to enhance the one-dimensional anisotropic fusion of cubic nanocrystals through an oriented-attachment mechanism. This coordination-modulation method was probed to produce highly crystalline microtubes of the Cu-MOF [Cu₂(ndc)₂(dabco)] (ndc = 1,4-naphthalenedicarboxylate, dabco = 1,4-diazabicyclo[2.2.2]octane) with high porosity, comparable to that of bulk crystals synthesized by the conventional solvothermal

[a] QuiMolMat Group, CICA, Department of Fundamental Chemistry, Faculty of Sciences, University of A Coruña, Campus A Coruña, 15071 A Coruña, Spain
E-mail: suqui@udc.es
<https://cica.udc.es/es/grupo/quimica-molecular-y-de-materiales>

[b] Department of Applied Physics, University of Santiago de Compostela, 15782 Santiago de Compostela, Spain

[c] Instituto Nacional del Carbón (INCAR-CSIC), Apartado 73, 33080 Oviedo, Spain

Supporting information and ORCID(s) from the author(s) for this article are available on the WWW under <http://dx.doi.org/10.1002/ejic.201600192>.

method. The strategy basically consists of the modulation of the coordination equilibrium through the simple addition of external capping reagents (modulators) with the same chemical functionality as the organic linkers to compete for the coordination of the metal ions.^[19] The generated competition regulates the rate of framework extension and crystal growth and, according to Tsuruoka et al.,^[19] allows the control of the resulting crystal morphology.

In this paper and with the same philosophy, we report the synthesis of a Co-MOF as a precursor for the synthesis of hollow Co₃O₄ microtubes. In our case, we used the MOF [Co₂(NH₂-bdc)₂(dabco)]·[G] [NH₂-bdc = 2-amino-1,4-benzenedicarboxylate anions, G = *N,N*-dimethylformamide (DMF) and H₂O], which is similar to the reported [Cu₂(ndc)₂(dabco)] but with the NH₂-bdc ligand instead of ndc. This Co-MOF was prepared readily as oriented and controlled hollow microtubes without the use of external modulators during the synthesis.

Results and Discussion

Synthesis

The Co-MOF [Co₂(NH₂-bdc)₂(dabco)]·[G] was prepared by a modification^[21] of the synthetic route previously reported for the preparation of [Zn₂(NH₂-bdc)₂(dabco)].^[22,23] The starting materials [Co(NO₃)₂·6H₂O, 2-NH₂-H₂bdc, and dabco] were dissolved in DMF, and the mixture was stirred at room temperature for 5 h. The mixture was then filtered to remove the precipitate. The solution was heated in a Teflon-lined autoclave at 393 K for 72 h, and the precipitate was washed with DMF and dried at room temperature to afford needle-shaped green crystals of [Co₂(NH₂-bdc)₂(dabco)]·[G]. Black crystals of Co₃O₄ were obtained readily through the thermal decomposition of the [Co₂(NH₂-bdc)₂(dabco)]·[G] crystals at 400 °C.

Thermal Decomposition of [Co₂(NH₂-bdc)₂(dabco)]·[G]

The thermogravimetric analysis (TGA) of [Co₂(NH₂-bdc)₂(dabco)]·[G] was performed to determine its stability and to control its thermal decomposition to the desired Co₃O₄ oxide. The Co-MOF undergoes two clear weight losses from room temperature to 350 °C (see Figure 1). The first weight loss of approx-

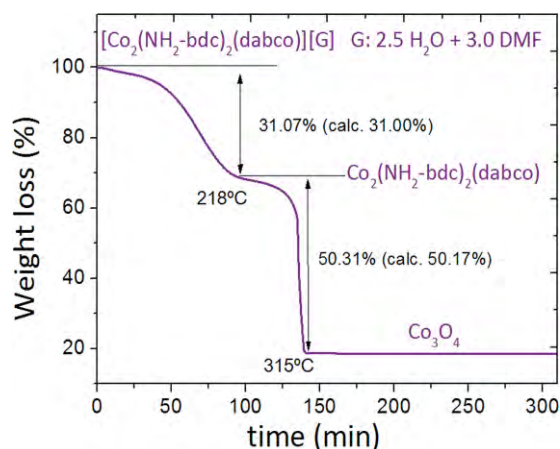


Figure 1. Thermogravimetric curve for [Co₂(NH₂-bdc)₂(dabco)]·[G] crystals measured under dry air.

imately 31 % (up to 218 °C) coincides with the calculated mass for 2.5 H₂O and 3.0 DMF guest molecules per formula. The last weight loss of approximately 50 % (in the interval 218–315 °C) is due to the decomposition of the framework to form Co₃O₄, as confirmed by the powder X-ray diffraction measurement of the residual sample after the thermal analysis (see Figure 2).

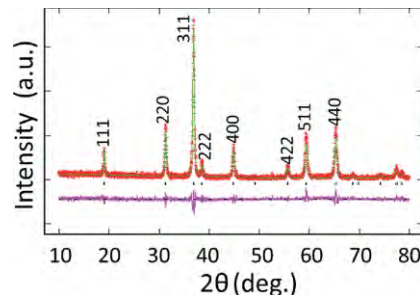


Figure 2. PXRD pattern of Co₃O₄. The pink line represents the difference between the experimental data (red points) and the data calculated by Rietveld refinement (green line).

Elemental Chemical Analysis and Infrared Spectroscopy

The chemical composition obtained by the C, N, and H elemental chemical analysis of [Co₂(NH₂-bdc)₂(dabco)]·[G] was C 44.32, H 4.98, N 11.89. These results fit quite well with the calculated C 43.66, H 5.67, N 11.49 for the 2.5 H₂O and 3.0 DMF guest molecules observed by TGA.

The FTIR spectrum of [Co₂(NH₂-bdc)₂(dabco)]·[G] (Figure S1, Supporting Information) is in good agreement with the literature data for [Co₂(bdc)₂(dabco)]·[G]^[24] and is consistent with the presence of NH₂-bdc and dabco ligands as well as H₂O and DMF guest molecules. The suggested assignments for the main observed bands of this spectrum are also provided in the Supporting Information.

Structural Characterization

Single-crystal X-ray diffraction (SCXRD) analysis at 100 K indicates that [Co₂(NH₂-bdc)₂(dabco)]·[G] crystallizes in the tetragonal space group *I4/mcm* with the cell parameters *a* = 15.194(5) Å and *c* = 19.105(5) Å. The crystal data as well as details of the data collection and refinement are summarized in Table 1 and Figure 3. The [Co₂(NH₂-bdc)₂(dabco)] framework consists of two-dimensional layers of Co₂ paddle wheels linked together by NH₂-bdc anions and dabco molecules, which act as pillar ligands to connect the square nets into a 3D host structure. The carbon atoms of the dabco molecules are disordered at different positions, and the amino groups are also disordered at the four possible different positions of each benzene ring. Such a framework displays a 3D interconnected pore system in which several DMF and H₂O polar guest species are located. As those guest species are highly disordered and could not be properly modeled, the SQUEEZE routine of PLATON^[25] was applied to remove their contributions to the scattering; therefore, the reported refinements are for the guest-free structure. We have to note that this crystal structure is very similar to those

reported for the related MOFs without the amino group in the bdc ligands, $[M_2(\text{bdc})_2(\text{dabco})]\cdot[G]$ ($M^{2+} = \text{Co}^{2+}, \text{Zn}^{2+}, G = \text{DMF}$ and H_2O);^[26,27] therefore, the presence of the $-\text{NH}_2$ groups does not seem to affect the reticulation process of these pillared MOFs.

Table 1. Single-crystal X-ray diffraction data of $[\text{Co}_2(\text{NH}_2\text{-bdc})_2(\text{dabco})]\cdot[G]$.

Empirical formula	$\text{C}_{11}\text{CoN}_2\text{O}_4$
Formula mass	283.16
Crystal system	tetragonal
$a/\text{\AA}$	15.194(5)
$b/\text{\AA}$	15.194(5)
$c/\text{\AA}$	19.105(5)
Unit cell volume / \AA^3	4411(2)
Temperature /K	100(2)
Space group	$I4/mcm$
Formula units per unit cell, Z	8
Radiation type	Mo- K_α
Independent reflections	382
Final R1 value [$I > 2\sigma(I)$]	0.0497
Final $wR(F^2)$ value [$I > 2\sigma(I)$]	0.1290
Final R1 value (all data)	0.0699
Final $wR(F^2)$ value (all data)	0.1378
Goodness of fit on F^2	1.074

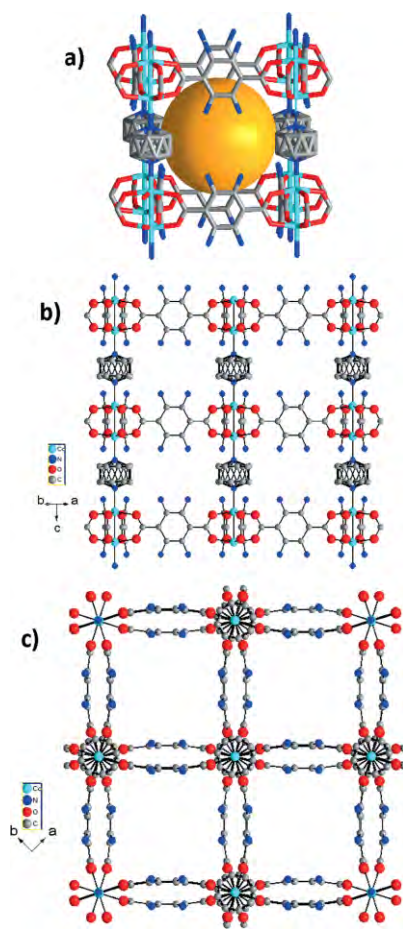


Figure 3. (a) Crystal structure of $[\text{Co}_2(\text{NH}_2\text{-bdc})_2(\text{dabco})]$ viewed along (b) the $[110]$ direction and (c) the $[001]$ direction. Hydrogen atoms are not represented. The carbon atoms of the dabco pillars and the NH_2 groups are disordered.

In addition, according to the powder X-ray diffraction (PXRD) data, the as-obtained $[\text{Co}_2(\text{NH}_2\text{-bdc})_2(\text{dabco})]\cdot[G]$ sample is single-phased, and good agreement was observed between the experimental data and the proposed model for the fitting (see Figure 4), except for the high intensity of the (110) and (220) diffraction maxima. This discrepancy proves that this MOF displays a marked preferred orientation owing to the growth of the crystals along the direction of the dabco pillars, which corresponds to the $[001]$ direction. The mentioned intensity differences could additionally be caused by the presence of guest molecules in the framework, as the simulated PXRD pattern is based on the guest-free framework, whereas the experimental PXRD pattern was collected for a partially solvated sample. However, we assume that the influence of the preferred orientation is more important, because of the high anisotropy of the crystals, as confirmed by SEM.

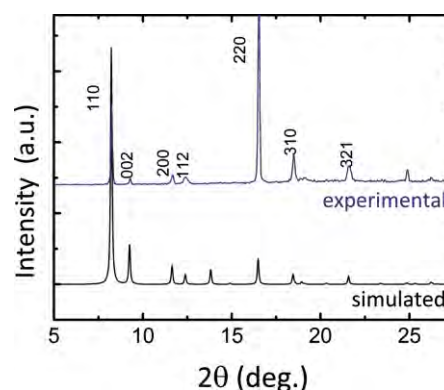


Figure 4. Experimental PXRD pattern of $[\text{Co}_2(\text{NH}_2\text{-bdc})_2(\text{dabco})]\cdot[G]$ compared with that simulated from the single-crystal X-ray diffraction data.

The PXRD pattern (Figure 2) indicates that pure and well-crystallized Co_3O_4 is obtained by simple calcination of the MOF. This material shows the expected normal spinel structure (space group $Fd\bar{3}m$) with a cell parameter $a = 8.0869(2)$ \AA . We have to note that this pattern displays considerable peak broadening, which is a sign of the nanometric size of the particles. From this peak broadening and by using the Debye-Scherrer equation, we have estimated that the average crystal size is ca. 33 nm.

Morphological Characterization

The SEM images of the as-obtained microcrystals of $[\text{Co}_2(\text{NH}_2\text{-bdc})_2(\text{dabco})]\cdot[G]$ are shown in Figure 5. As can be seen in Figure 5a, this MOF crystallizes as square rods with different sizes, namely, (1) hollow microtubes with lengths on the mm scale and ca. 40 μm thick (detail in Figure 5b) and (2) square rods ca. 100 μm long and ca. 5 μm thick (detail in Figure 5c–e). The magnification of these images reveals that all of these rods are in turn formed by nanotubes ca. 200 nm thick and aligned perfectly together (see details in Figure 5d–f). Moreover, as shown in Figure 5e–g, small quantities of quite regular spherical particles in the 2 μm (detail in Figure 5e and f) and 200 nm ranges (see detail in Figure 5g) are also present. Very interestingly, the nanotubes tend to aggregate to form hollow tubes with open

ends and very regular cavities. This tendency is observed in the bigger tubes (Figure 5b) but also in the smaller ones (Figure 5e).

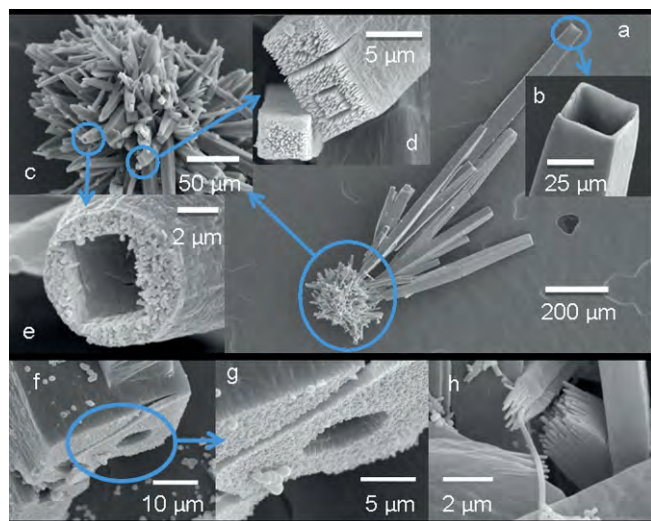


Figure 5. SEM micrographs of $[\text{Co}_2(\text{NH}_2\text{-bdc})_2(\text{dabco})]\cdot[\text{G}]$ crystals; (b)–(e) magnifications of selected regions indicated in blue in (a) and (c); (f) and (h) magnifications of other regions in (c).

The morphology of the Co_3O_4 obtained by the calcination of the MOF is shown in Figures 6 and S2. The Co_3O_4 crystals preserve the hollow tubular morphology and the compactness of the tubular walls of the precursor. The main difference compared with the parent MOF is a slight contraction of the crystal walls (see detail in Figure 6c). Moreover, it can be clearly seen by TEM that even the smaller tubes are hollow and very regular with diameters of ca. 200 nm and walls ca. 20–30 nm thick (Figure S2).

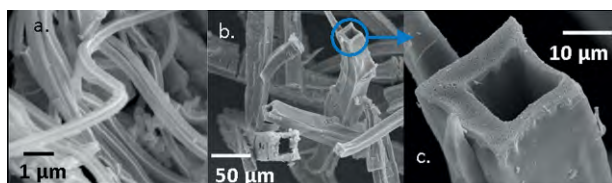


Figure 6. SEM micrographs of the obtained Co_3O_4 material.

Gas Adsorption–Desorption

The N_2 adsorption–desorption isotherms of crystalline MOF microtubes at 77 K are shown in Figure 7. The pore sizes are generally below 2 nm (so-called micropores), and the Brunauer–Emmett–Teller (BET) surface area is as large as $1518 \text{ m}^2/\text{g}$. Notably, the specific surface area of the Co-MOF microtubes is comparable to that of the analogous Zn-MOF $[\text{Zn}_2(\text{NH}_2\text{-bdc})_2(\text{dabco})]$ ^[22] and clearly larger than that of the nanostructured Cu-MOF $[\text{Cu}_2(\text{ndc})_2(\text{dabco})]$ prepared by a similar technique but with an external modulator.^[19,20]

Additionally, the N_2 adsorption–desorption isotherms of Co_3O_4 at 77 K are shown in Figure S3. These isotherms show hysteresis in the large P/P_0 range of ca. 0.8–1.0, which indicates the presence of mesopores in the oxide crystals, whereas the

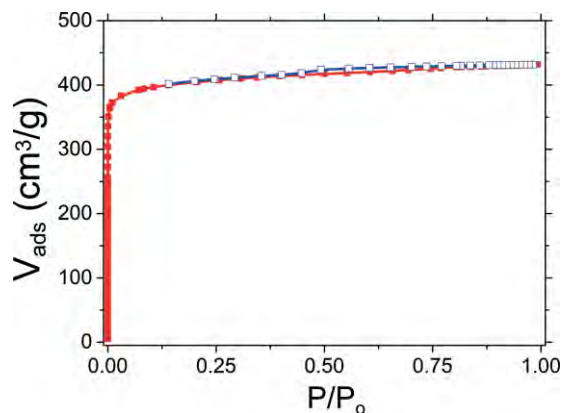


Figure 7. Gas adsorption (red solid symbols) and desorption (blue open symbols) isotherms of N_2 at 77 K for $[\text{Co}_2(\text{NH}_2\text{-bdc})_2(\text{dabco})]$ crystals.

measured BET surface area of $31 \text{ m}^2/\text{g}$ is in the range reported for similar nanostructured Co_3O_4 materials.^[17]

Crystal Formation and Growth

The results show that the $[\text{Co}_2(\text{NH}_2\text{-bdc})_2(\text{dabco})]\cdot[\text{G}]$ crystal growth is enhanced along one direction, and this results in the formation of hollow microtubes, similarly to the previously reported synthesis of the related MOF $[\text{Cu}_2(\text{ndc})_2(\text{dabco})]$.^[19,20] The formation of the hollow microtube crystals also appears to occur in two steps: (1) the formation of nanoparticles and (2) the anisotropic aggregation of these nanoparticles along a unique preferential direction. As we have shown above, the microphotographs of the Co-MOF obtained by SEM (see Figure 5e–g) show the presence of some spherical nanoparticles with diameters in the 2 μm and 200 nm ranges in addition to the microtubes. The previously proposed growth mechanism for $[\text{Cu}_2(\text{ndc})_2(\text{dabco})]$ ^[19] consisted of the growth of microtubes as nanorods along the [001] direction of the tetragonal framework system, that is, along the dabco–cobalt coordination direction, presumably because of the presence of an external capping reagent (modulator), acetic acid, which has the same carboxylate functionality as the ndc and impedes the ndc–copper interaction.^[19,20] In our case, as we avoided the use of an external modulator reagent, the amino groups of the bdc ligands could enhance the one-dimensional anisotropic aggregation of the nanocrystals through an oriented attachment.

Moreover, we have compared the $[\text{Co}_2(\text{NH}_2\text{-bdc})_2(\text{dabco})]\cdot[\text{G}]$ crystals with those of the analogous $[\text{Co}_2(\text{bdc})_2(\text{dabco})]\cdot[\text{G}]$ (without the NH_2 substituents) obtained by a similar synthetic method in our laboratory (Figure S4). We also observed the formation of $[\text{Co}_2(\text{bdc})_2(\text{dabco})]\cdot[\text{G}]$ microtubes. However, in contrast with those of $[\text{Co}_2(\text{NH}_2\text{-bdc})_2(\text{dabco})]\cdot[\text{G}]$, these microtubes are not hollow and, very importantly, their walls are formed by the aggregation of unaligned nanocrystals; consequently, they are much less compact. The different morphologies of $[\text{Co}_2(\text{bdc})_2(\text{dabco})]\cdot[\text{G}]$ and $[\text{Co}_2(\text{NH}_2\text{-bdc})_2(\text{dabco})]\cdot[\text{G}]$ could be a consequence of the different growth mechanisms of the crystals and confirm the role of the amino groups of the bdc ligands on the formation of hollow microstructures.

Magnetic Properties of Co₃O₄

Bulk Co₃O₄ presents a cubic (A)₂(B)₂O₄ normal spinel structure, in which the diamagnetic low-spin Co³⁺ ions are at the octahedral sites; the spin moments of the Co²⁺ ions at the tetrahedral sites exhibit antiferromagnetic ordering at $T < T_N$ ($T_N = 40$ K), and each Co²⁺ ion is surrounded by four nearest-neighbor Co²⁺ ions with oppositely directed spins.^[28]

The temperature dependence of the molar magnetic susceptibility χ_m of the nanostructured Co₃O₄ material recorded under an applied magnetic field of 1000 Oe in zero-field-cooled (ZFC) and field-cooled (FC) conditions is shown in Figure 8. The general aspect of the curves is quite similar to those observed for other nanoparticulate Co₃O₄ systems, and they show^[1,29] (1) the paramagnetic behavior of the material from room temperature down to 34 K, (2) the maxima in both the ZFC and FC χ_m data at $T = 34$ K that corresponds to the Néel transition to the antiferromagnetic (AFM) state, (3) the splitting of the FC and ZFC curves below 29 K, and (4) the slight increase of the FC susceptibility as the temperature decreases below 6 K.

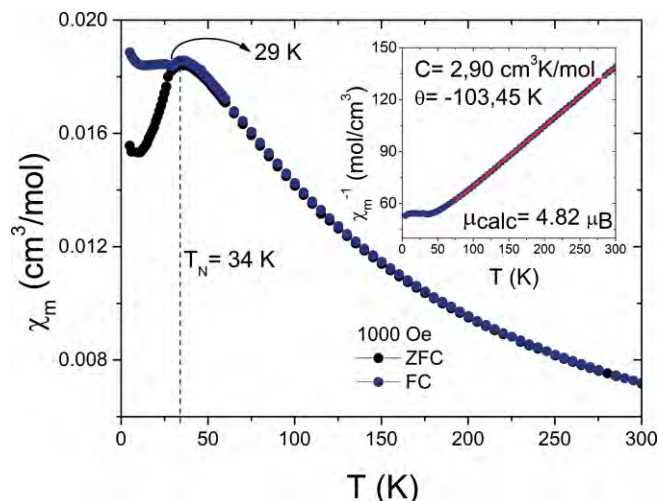


Figure 8. Temperature dependence of the ZFC and FC molar magnetic susceptibility (χ) of Co₃O₄ crystals measured in a field of 1000 Oe. Inset: the $1/\chi$ versus T curve, in which the solid line represents the fit obtained by the Curie–Weiss law.

The AFM interaction present in the Co₃O₄ nanotubes can also be verified by the plot of $1/\chi_m$ versus T (see inset in Figure 8). The molar magnetic susceptibility obeys the Curie–Weiss law in the temperature interval 70–300 K with a negative Weiss constant of $\theta = -103$ K and a Curie constant of $C = 2.90$ cm³ K/mol to yield an effective magnetic moment of $4.8 \mu_B$ per Co²⁺ ion. This effective magnetic moment is still higher than the expected value of $3.25 \mu_B$ found by neutron diffraction experiments^[28] even though it is much closer to it than those of other nanoparticulate Co₃O₄ materials, which exhibit much higher values (ca. 6–8 μ_B).^[2,5,30] In those latter systems, such large values have been attributed to the magnetic moment of Co³⁺ ions owing to defects in the materials such as nonstoichiometry in oxygen, the distortion of the crystal symmetry and lattice parameters because of the downsizing of the particles, and so forth.^[31] Our results could be considered as evidence for the quality of our system in terms of its crystalline symmetry.

The obtained Néel temperature of 34 K is slightly lower than that of 40 K for macroscopic Co₃O₄ crystals.^[29] This reduction in T_N as well as the splitting of the FC and ZFC curves below 29 K and the increase of the susceptibility for FC below 6 K are characteristic of nanostructured materials and can be understood in terms of a core–shell model with antiferromagnetic cores and weak ferromagnetic shells. According to this model, the latter arise from uncompensated magnetic moments at the surface of the particles. In this context, we can consider the magnetic behavior of our Co₃O₄ crystals as evidence of its nanostructured morphology with well-ordered cores and slightly magnetically disordered shells.^[31–34]

Conclusions

We successfully synthesized the Co-MOF [Co₂(NH₂-bdc)₂(dabco)]·[G] by a coordination-modulation method and elucidated its crystal structure by single-crystal X-ray diffraction. By SEM analysis, we verified that this Co-MOF grew readily with a complex microstructure, consisting of hollow microtubes with lengths in the scale of millimeters and ca. 40 μ m thick as well as square rods ca. 100 μ m long and ca. 5 μ m thick. We even observed that the walls of the hollow microtubes are formed through the aggregation of thinner nanotubes.

By the simple calcination of [Co₂(NH₂-bdc)₂(dabco)]·[G] at 400 °C, we successfully synthesized Co₃O₄ crystals, and the good crystallinity of the so-obtained oxide was confirmed by PXRD. The Co₃O₄ crystals show magnetic signatures typical of nanostructured Co₃O₄. SEM and TEM showed that the oxide is formed by hollow microtubes, and the peculiar nanostructured morphology of the original Co-MOF is maintained. This peculiar morphology gives interesting properties to both materials, such as large BET surface areas.

In summary, this work shows how the coordination-modulation method provides a simple route for the preparation of a nanostructured Co-MOF that can act as precursor to nanostructured Co₃O₄ and opens a way to the preparation of new oxides with controlled microstructures and advanced properties.

Experimental Section

Materials: All chemicals were commercially available and used without further purification.

[Co₂(NH₂-bdc)₂(dabco)]·[G]: Co(NO₃)₂·6H₂O (0.3492 g, 1.2 mmol), 2-NH₂-H₂bdc (0.2174 g, 1.2 mmol), and dabco (0.2131 g, 1.9 mmol) were dissolved separately in DMF (10 mL) to give purple, yellow, and colorless solutions, respectively. A green precipitate appeared when the dabco solution was added to the other two solutions. The mixture was stirred at room temperature for 5 h and then filtered to remove the precipitate. The solution was heated in a Teflon-lined autoclave at 393 K for 72 h and then filtered after slow cooling overnight, and the precipitate was washed with DMF and dried at room temperature. Green needle-shaped crystals of [Co₂(NH₂-bdc)₂(dabco)]·[G] (0.3 g, yield 30.5 %) were obtained.

Co₃O₄: Crystals of Co₃O₄ were obtained by the thermal decomposition of [Co₂(NH₂-bdc)₂(dabco)]·[G] in air at 400 °C for 4 h.

Physical Techniques: The PXRD patterns were collected at room temperature with a Siemens D-5000 diffractometer with Cu-K α radi-

ation ($\lambda = 1.5418 \text{ \AA}$) and analyzed by Le Bail profile analysis, and Rietveld refinement was performed with the FULLPROF^[35] and EXPGUI-GSAS software.^[36,37] The average crystallite size of Co_3O_4 was estimated from X-ray diffraction line broadening by using the Debye–Scherrer equation. The instrumental broadening was determined with LaB_6 powder (NIST SRM660a). The SCXRD data set for the Co-MOF at 100 K was collected with a Bruker Kappa ApexII X-ray diffractometer equipped with a CCD detector with monochromatic $\text{Mo-K}_{\alpha 1}$ radiation ($\lambda = 0.71073 \text{ \AA}$). A suitable crystal of approximately $0.07 \times 0.09 \times 0.31 \text{ mm}$ was mounted on a MiTeGen MicroMount™ using FOMBLIN® YR-1800 perfluoropolyether (Lancaster Synthesis). For these experiments, the crystal was cooled at different rates with a nitrogen cold stream from an Oxford Cryosystem cooler. The data integration and reduction were performed with the APEX2 V2013.2-0 (Bruker AXS, 2013) software suite. The intensity data were corrected for Lorentz and polarization effects and for absorption by semiempirical methods on the basis of symmetry-equivalent data with the SADABS 2012/1 software suite. The structure was solved by direct methods with SHELXS^[38] and refined by the least-squares method with SHELXL.^[38]

The morphologies of the samples were examined by SEM with a Jeol JSM 6400 microscope and by TEM with a JEOL 1010 microscope operating at 100 kV.

The TGA was performed with an SDT2960 TGA-DTA instrument. The sample (ca. 25 mg) was heated in a corundum crucible under a dry-air flow from room temperature to 800 °C at a rate of 5 K/min.

The IR spectra of the powdered products and the gases evolved during the TGA analyses were recorded with a Bruker Vector 22 FTIR spectrometer over the wavenumber range 400–4000 cm^{-1} .

Elemental chemical analyses for C, N, and H were performed with a FLASHEA1112 (Thermo-Finnigan) analyzer.

The porosities of the materials were examined through N_2 physisorption at 77 K (Micromeritics ASAP 2010). The sample (80–100 mg) was evacuated at room temperature for 5 h and subsequently outgassed at 105 °C for 15 h. The sample tubes were reweighed to obtain a consistent mass for the degassed modified samples, and then the adsorption–desorption isotherms were recorded. The specific surface areas were determined by the analysis of the adsorption branch of the isotherm with the BET equation.

The magnetic measurements were performed with a Quantum Design MPMS superconducting quantum interference device (SQUID) magnetometer. The ZFC and FC magnetic susceptibility data were obtained under a magnetic field of 1000 Oe in the temperature range $5 \leq T \leq 300 \text{ K}$.

Further details of the crystal structure investigation(s) may be obtained from Fachinformationszentrum Karlsruhe, 76344 Eggenstein-Leopoldshafen, Germany (fax: +49-7247-808-666; e-mail: crys-data@fiz-karlsruhe.de), on quoting the deposition number CSD-426918.

Supporting Information (see footnote on the first page of this article): TEM micrographs of the obtained Co_3O_4 material and SEM micrographs of $[\text{Co}_2(\text{bdc})_2(\text{dabco})] \cdot [\text{G}]$ crystals.

Acknowledgments

The authors are grateful for the financial support from the Ministerio de Economía y Competitividad (MINECO) (ENE2014-56237-C4-4-R) and the Xunta de Galicia under the project GRC2014/042. L. C. G-A. also wants to thank the University of A

Coruña (UDC) for a predoctoral fellowship, J. M. B-G. wants to thank the Barrié Foundation for a predoctoral fellowship, and S. Y-V. wants to thank the Xunta de Galicia for a postdoctoral grant (Plan I2C).

Keywords: Crystal growth · Metal–organic frameworks · Microporous materials · Nanotubes · Cobalt

- [1] G. Wang, X. Shen, J. Horvat, B. Wang, H. Liu, D. Wexler, J. Yao, *J. Phys. Chem. C* **2009**, *113*, 4357–4361.
- [2] X. Wang, W. Tian, T. Zhai, C. Zhi, Y. Bando, D. Golberg, *J. Mater. Chem.* **2012**, *22*, 23310–23326.
- [3] Y. Lu, Y. Wang, Y. Zou, Z. Jiao, B. Zhao, Y. He, M. Wu, *Electrochem. Commun.* **2010**, *12*, 101–105.
- [4] S. Choi, B. Min, *Sens. Actuators B* **2001**, *77*, 330–334.
- [5] X.-P. Shen, H.-J. Miao, H. Zhao, Z. Xu, *Appl. Phys. A* **2008**, *91*, 47–51.
- [6] S. Sharma, N. Garg, K. V. Ramanujachary, S. E. Lofland, A. K. Ganguly, *Cryst. Growth Des.* **2012**, *12*, 4202–4210.
- [7] C. Xiang, M. Li, M. Zhi, A. Manivannan, N. Wu, *J. Power Sources* **2013**, *226*, 65–70.
- [8] O. M. Yaghi, M. O’Keeffe, N. W. Ockwig, H. K. Chae, M. Eddaoudi, J. Kim, *Nature* **2003**, *423*, 705–714.
- [9] A. K. Cheetham, C. N. R. Rao, *Science* **2007**, *318*, 58–59.
- [10] W. Zhang, R.-G. Xiong, *Chem. Rev.* **2012**, *112*, 1163–1195.
- [11] G. C. Xu, W. Zhang, X. M. Ma, Y. H. Chen, L. Zhang, H. L. Cai, Z. M. Wang, R. G. Xiong, S. Gao, *J. Am. Chem. Soc.* **2011**, *133*, 14948–14951.
- [12] P. Jain, V. Ramachandran, R. J. Clark, H. D. Zhou, B. H. Toby, N. S. Dalal, H. W. Kroto, A. K. Cheetham, *J. Am. Chem. Soc.* **2009**, *131*, 13625–13627.
- [13] T. K. Kim, K. J. Lee, J. Y. Cheon, J. H. Lee, S. H. Joo, H. R. Moon, *J. Am. Chem. Soc.* **2013**, *135*, 8940–8946.
- [14] X. Ge, Z. Li, C. Wang, L. Yin, *ACS Appl. Mater. Interfaces* **2015**, *7*, 26633–26642.
- [15] H. Yu, H. Fan, B. Yadian, H. Tan, W. Liu, H. H. Hng, Y. Huang, Q. Yan, *ACS Appl. Mater. Interfaces* **2015**, *7*, 26751–26757.
- [16] K. J. Lee, T.-H. Kim, T. K. Kim, J. H. Lee, H.-K. Song, H. R. Moon, *J. Mater. Chem. A* **2014**, *2*, 14393–14400.
- [17] Y. Han, M. Zhao, L. Dong, J. Feng, Y. Wang, D. Li, X. Li, *J. Mater. Chem. A* **2015**, *3*, 22542–22546.
- [18] C. Li, T. Chen, W. Xu, X. Lou, L. Pan, Q. Chen, B. Hu, *J. Mater. Chem. A* **2015**, *3*, 5585–5591.
- [19] T. Tsuruoka, S. Furukawa, Y. Takashima, K. Yoshida, S. Isoda, S. Kitagawa, *Angew. Chem. Int. Ed.* **2009**, *48*, 4739–4743; *Angew. Chem.* **2009**, *121*, 4833.
- [20] M.-H. Pham, G.-T. Vuong, F.-G. Fontaine, T.-O. Do, *Cryst. Growth Des.* **2012**, *12*, 3091–3095.
- [21] M. Sánchez-Andújar, S. Yáñez-Vilar, B. Pato-Doldán, C. Gómez-Aguirre, S. Castro-García, M. A. Señarís-Rodríguez, *J. Phys. Chem. C* **2012**, *116*, 13026–13032.
- [22] Z. Wang, K. K. Tanabe, S. M. Cohen, *Inorg. Chem.* **2009**, *48*, 296–306.
- [23] H. Chun, D. N. Dybtsev, H. Kim, K. Kim, *Chem. Eur. J.* **2005**, *11*, 3521–3529.
- [24] H. Wang, J. Getzschmann, I. Senkowska, S. Kaskel, *Microporous Mesoporous Mater.* **2008**, *116*, 653–657.
- [25] A. L. Spek, *Acta Crystallogr., Sect. D: Biol. Crystallogr.* **2009**, *65*, 148–155.
- [26] H. Wang, J. Getzschmann, I. Senkowska, S. Kaskel, *Microporous Mesoporous Mater.* **2008**, *116*, 653–657.
- [27] A. J. Fletcher, K. M. Thomas, M. J. Rosseinsky, *J. Solid State Chem.* **2005**, *178*, 2491–2510.
- [28] W. L. Roth, *J. Phys. Chem. Solids* **1964**, *25*, 1–10.
- [29] P. Dutta, M. S. Seehra, S. Thota, J. Kumar, *J. Phys. Condens. Matter* **2008**, *20*, 1–8.
- [30] Y. Ichianagi, S. Yamada, *Polyhedron* **2005**, *24*, 2813–2816.
- [31] M. J. Benitez, O. Petravic, E. L. Salabas, F. Radu, H. Tüysüz, F. Schüth, H. Zabel, *Phys. Rev. Lett.* **2008**, *101*, 97206–97209.
- [32] T. Ambrose, C. Chien, *Phys. Rev. Lett.* **1996**, *76*, 1743–1746.
- [33] L. He, C. Chen, N. Wang, W. Zhou, L. Guo, *J. Appl. Phys.* **2007**, *102*, 103911.

- [34] X. Zheng, C. Xu, K. Nishikubo, K. Nishiyama, W. Higemoto, W. Moon, E. Tanaka, E. Otake, *Phys. Rev. B* **2005**, *72*, 014464–014471.
- [35] J. Rodríguez-Carvajal, *CPD Newsletter* **2001**, *26*, 12–19.
- [36] B. H. Toby, *J. Appl. Crystallogr.* **2001**, *34*, 210–213.
- [37] A. C. Larson and R. B. Von Dreele, *General Structure Analysis System (GSAS)*, **1994**, Report LAUR 86–748.
- [38] G. M. Sheldrick, *Acta Crystallogr., Sect. A: Found. Crystallogr.* **2008**, *64*, 112–122.

Received: February 25, 2016

Published Online: July 4, 2016